

NASA TECHNICAL NOTE



NASA TN D-4690

C.1

NASA TN D-4690



LOAN COPY: RETURN TO
AFWL (WLDL-2)
KIRTLAND AFB, N MEX

TURBOJET-ENGINE NOISE STUDIES TO EVALUATE EFFECTS OF INLET-GUIDE-VANE—ROTOR SPACING

by John L. Crigler, W. Latham Copeland, and Garland J. Morris
Langley Research Center
Langley Station, Hampton, Va.

NATIONAL AERONAUTICS AND SPACE ADMINISTRATION • WASHINGTON, D. C. AUGUST 1968





TURBOJET-ENGINE NOISE STUDIES TO EVALUATE EFFECTS
OF INLET-GUIDE-VANE—ROTOR SPACING

By John L. Crigler, W. Latham Copeland,
and Garland J. Morris

Langley Research Center
Langley Station, Hampton, Va.

NATIONAL AERONAUTICS AND SPACE ADMINISTRATION

TURBOJET-ENGINE NOISE STUDIES TO EVALUATE EFFECTS OF INLET-GUIDE-VANE—ROTOR SPACING

By John L. Crigler, W. Latham Copeland,
and Garland J. Morris
Langley Research Center

SUMMARY

Some experimental results are presented of a noise study which made use of a turbojet engine having an axial-flow multiple-stage compressor. The objective of this study was to investigate the effect of increased inlet-guide-vane—rotor spacing on the compressor interaction noise and engine performance, particularly at partial-power conditions. The engine selected for this investigation was in the 2000-pound (8896-newton) thrust category and was readily modified by relocating the inlet-guide-vane assembly approximately six mean rotor-blade chords ahead of the first-stage rotor.

The data are presented in the form of engine-performance curves, noise-radiation patterns, and frequency spectra. The data show that there is a substantial noise reduction due to the increased inlet-guide-vane—first-stage-rotor axial spacing. The reductions were as much as 14 dB for the condition of 80-percent rated rpm, the highest engine speed at which noise measurements were made. The noise reductions have been accomplished without any measurable loss in engine performance. Stationary components of the compressor which are exposed to pulsating flows are identified as sources of noise and are noted to have characteristic frequencies.

INTRODUCTION

One of the principal sources of noise in axial-flow compressors is due to the aerodynamic interactions between the stationary vanes and rotating blades. These interactions produce discrete tones which are of major concern in landing-approach conditions. Experimental studies conducted with a single-stage axial-flow compressor consisting of inlet guide vanes (IGV) and rotor have shown that an increased spacing between the IGV and rotor resulted in a substantial reduction in the discrete tone of the compressor. (See ref. 1.) The tests in reference 2 extended the experimental work of reference 1 to include the effect of the downstream stator on the interaction noise of the rotor-stator combination as well as the IGV-rotor-stator combination. The study in reference 2 showed the noise due to the interactions of the rotor and downstream stator to be appreciably less

than that due to the IGV and rotor interactions. Furthermore, the noise reductions obtained by increasing the spacing between the IGV and rotor were found to be relatively independent of the presence of the downstream stator.

In view of the encouraging results from the tests with a single-stage compressor in references 1 and 2, the IGV-rotor spacing of the compressor of a turbojet engine in the 2000-pound (8896-newton) thrust category was increased with the objective of evaluating the noise reductions and associated engine performance. The only change was to relocate the IGV assembly of the compressor approximately six mean rotor-blade chords ahead of the first-stage rotor.

The engine was instrumented to measure the pertinent performance parameters, and was operated over a range of speeds from 35-percent to 100-percent rated rpm. Far-field noise measurements were made at azimuth angles from near 0° (in front) to 90° from the thrust axis. Acoustic and performance data for both the standard and modified engine are presented herein.

SYMBOLS

B	number of rotor blades
F_n	engine net thrust, pounds (newtons)
f	frequency, hertz
K	index (. . . -1, 0, 1, 2 . . .)
$K'_{m\mu}$	characteristic wave number
M_m	circumferential tip Mach number for m-lobe pattern
M_m^*	cut-off Mach number
M_t	rotor-tip Mach number
m	lobe number ($m = nB + KV$)
N	rotor-shaft speed, revolutions per minute or revolutions per second
n	harmonic number

V	number of vanes
W_f	engine fuel flow, pounds per hour (kilograms per hour)
δ	ratio of total pressure to 2116 pounds per square foot (101 314 newtons per square meter)
θ	ratio of total temperature to 15° C
μ	radial mode index
ξ	cut-off ratio M_m/M_m^*

Engine-performance parameters for standard sea-level condition:

F_n/δ	corrected engine thrust, pounds (newtons)
$N/N_{std}\sqrt{\theta}$	corrected engine speed, percent rated rpm

Subscripts:

R	rotor
S	stator
0	IGV
1,2 . . .	stator or rotor stage number

APPARATUS AND METHODS

Description of Engine and Installation

A turbojet engine, incorporating a seven-stage axial-flow compressor, was mounted on an outdoor thrust stand for the investigation. The engine is rated for take-off at 1750 pounds (7784 newtons) maximum thrust at 13 800 rpm, and the design airflow is 32 lb/sec (14.5 kg/sec) at standard sea-level conditions, 2116 lb/ft² (101 314 N/m²) intake pressure and 15° C temperature.

The compressor inlet-guide-vane assembly had 41 vanes with a constant chord of 1.00 inch (25.4 mm). The first-stage rotor had 29 blades with a root chord of 1.75 inches (44.45 mm) and a tip chord of 1.25 inches (31.75 mm), which gave a mean chord of 1.50 inches (38.10 mm). The general arrangement of the IGV relative to the first-stage rotor is shown in figure 1. In the standard configuration, the IGV assembly was installed

approximately one-eighth mean rotor-blade chord ahead of the first-stage rotor. Three struts (fig. 1) 120° apart were located approximately two mean rotor-blade chords upstream of the rotor. These struts had a constant chord of 6.0 inches (152.4 mm) and supported the bearings and gears. The relatively simple modification entailed moving the IGV assembly ahead of the struts and fitting in its place a spacer or separation ring. This modification resulted in an IGV-rotor separation of approximately six mean rotor-blade chords, as shown in figure 1. The same strut configuration and inlet duct were used for the standard and modified engine.

Noise Measurements and Instrumentation

The noise measurements were made in accordance with recommendations of reference 3. These measurements were obtained along a 25-foot-radius (7.62-meter) azimuth circle from 0° (ahead of inlet) to 90° and were continuously recorded with a moving microphone that traversed the azimuth range. In addition, this microphone was used to obtain 1.0-minute noise recordings for stationary conditions at the 0° , 15° , 30° , 45° , and 60° azimuth positions. The tests were conducted in an open area with no reflecting surfaces within several hundred feet, other than the ground which was concrete. The microphone was located about 6.0 feet (1.83 meters) above the ground level in the horizontal plane containing the engine center line. Figure 2 is a sketch of the noise-measuring area. A condenser microphone was used and the output signal was recorded on one channel of a multichannel tape recorder. The overall response of the system from 20 hertz to 15 000 hertz was flat within ± 2 dB.

Compressor-Performance Instrumentation

Instrumentation was provided for measuring various parameters necessary for determining engine performance during test operations. Included were devices for indicating engine rotational speed, exhaust-gas temperature, overall thrust, fuel flow, inlet air temperature, and outlet air temperature and pressure. Also, pitot-static tubes were installed in the compressor inlet duct and connected to a manometer board in order to obtain data from which inlet air velocity and weight flow were computed.

Operating Procedures

The engine in both the standard and modified configurations was operated over a range of speeds in order to investigate the effects of increased IGV-rotor spacing on the noise radiated out the inlet duct. Noise data were obtained over the range of engine rpm from 35 percent to 80 percent, corresponding to landing-approach conditions, and performance data were obtained over the range of engine rpm from 35 percent to 100 percent. Ambient air pressures and temperatures were obtained from the local weather station.

RESULTS AND DISCUSSION

Effects of IGV-Rotor Spacing on Performance

The performance data for both the standard and modified configurations have been corrected to standard atmosphere, and the pertinent parameters are plotted in figure 3 as a function of corrected engine rpm. The differences found as a result of the modification indicated a slight improvement in the overall engine performance. For the modified engine, a slightly higher thrust (fig. 3(a)) and the same or a slightly lower specific fuel consumption (fig. 3(b)) were indicated at all engine speeds. The weight flow of air through the compressor is shown to be relatively unchanged by the modification at all engine speeds. (See fig. 3(c).) These results suggest that the engine performance is not significantly changed by the increased IGV-rotor spacing.

Effects of IGV-Rotor Spacing on Noise Generation

The noise data obtained in this study are presented in figures 4 to 10 and are in the form of noise-radiation patterns and frequency spectra for both the standard and modified engine.

Overall-noise-radiation patterns.- In figure 4 are plotted the overall-noise-radiation patterns as a function of azimuth angle (0° to 90°) for the standard and modified engine, as obtained from a moving microphone. Since these measurements were taken in the forward quadrant, no attempt was made to separate the exhaust noise from the overall noise. Figure 4(a) shows data for 35-percent rated rpm; 4(b), for 60-percent rated rpm; and 4(c), for 80-percent rated rpm. It is seen that for the engine speeds for which data are presented, as the engine speed is increased, the overall-noise level increases over the entire azimuth range. The effects of increased IGV-rotor spacing are represented by the differences in sound pressure level between the two curves for each operating speed. There are substantial noise reductions over the entire azimuth range for all three engine speeds because of the increased IGV-rotor spacing, the greatest reduction in the overall noise being approximately 14 dB for an engine speed of 80-percent rated rpm.

Noise spectra.- Figure 5 presents one-third-octave band spectra of the noise for both the standard and modified engine, as measured at two different azimuth locations for an engine speed of 80-percent rated rpm (same condition as in fig. 4(c)). Figure 5(a) compares the spectra for the standard and modified engine, as measured at 30° azimuth, and is seen to contain both broad-band and discrete frequency components. The modified engine, incorporating increased IGV-rotor spacing, has lower noise levels over the entire spectrum. The results presented in figure 5(a) are typical of the measured data for other azimuth angles, as shown by the data in figure 5(b) for the 60° azimuth angle.

From an inspection of the spectra of figure 5, it can be seen that several distinct peaks occur in the frequency range above about 5000 hertz. Narrow-band analyses have been performed to define these peaks in more detail and are presented in figure 6. These frequency analyses made use of a one-tenth-octave band filter and were performed over the frequency range of 3000 hertz to 15 000 hertz. The data shown in the figure are for the 30° azimuth location and 80-percent engine speed (11 040 rpm) for both the standard engine (solid curve) and the modified engine (dashed curve). The curve for the standard engine shows the noise levels relative to the maximum noise peak, which occurs at a frequency of approximately 5300 hertz and corresponds to the first-stage-rotor fundamental blade-passage frequency B_1N . Another distinct peak of nearly the same magnitude appears at approximately 10 600 hertz, which corresponds to the first-stage-rotor second harmonic $2B_1N$. A third peak, which is identifiable but at a lower noise level (approximately 10 dB lower) than the other two, occurs at approximately 7900 hertz, which corresponds to the second-stage-rotor fundamental blade-passage frequency B_2N . As was pointed out in references 1 and 2, these discrete frequencies are strengthened by aerodynamic interactions of the stationary vanes and rotating blades of the compressor. With increased spacing, the aerodynamic interactions tend to be weakened, and thus it would be expected that the associated noise level would decrease.

The data for the modified engine (dashed curve) show large noise reductions over the entire spectrum. Of particular interest are the almost complete eliminations of the peaks at 7900 hertz (B_2N) and at 10 600 hertz ($2B_1N$). It can be seen that for this rpm and azimuth angle, the major source of the forward radiated noise from either the standard or modified engine results from the tones of the first-stage rotor.

It should be noted that the three struts in the inlet generate wakes in which the rotors must operate. Removal of the struts or moving them ahead of the IGV might further reduce the noise, although the results of this study suggest that these rotor-strut interactions are not very effective in generating noise.

Noise-radiation patterns at first-stage-rotor fundamental frequency.- Data in the form of radiation patterns for the first-stage-rotor fundamental frequency are presented in figure 7. Radiation patterns for both the standard and modified engine are included for the 80-percent speed condition (same condition as in fig. 6). Substantial noise-level reductions due to increased IGV-rotor spacing were obtained at all azimuth angles. It is significant that the major source of the overall noise at this and higher speeds occurs at the fundamental first-stage-rotor frequency B_1N . For lower engine speeds, however, somewhat different results have been obtained, as will be shown in the following section.

Special Effects Associated With Engine Speed

At 60-percent and 35-percent engine speeds, discrete frequency components other than those associated with the fundamental blade-passage frequency of the first rotor were found to be important for this engine. This phenomenon is illustrated in figures 8 and 9, where data are shown for the 30° azimuth location for these two engine speeds.

These data were obtained from an analysis using a 50-hertz constant-bandwidth filter over a frequency range of 2000 hertz to 9000 hertz. It can be seen that several distinct peaks occur in the spectra. The peaks associated with the rotor have been identified in the figures. In contrast to the case of 80-percent rated rpm for the standard engine, where the fundamental frequency of the first-stage rotor B_1N predominates (fig. 6), for the lower speeds the fundamental frequency of the second-stage rotor B_2N is the most intense component. In order to explain the shift of the relative importance from the first-stage rotor at 80-percent speed to the second-stage rotor at the lower speeds, it is helpful to study the duct transmission phenomena of the spinning modes and the "cut-off" concept which is described below.

Decay of spinning modes in the inlet duct.- In reference 4, it is shown that the rotor-stator interaction noise consists of many "spinning-mode" patterns of a single frequency, each pattern having a number of lobes and a rotational speed which can be specified as $\frac{NB}{m}$, where N is the shaft rotational speed, B is the number of blades, and m is the number of lobes. The value of m in a particular rotor-generated spinning-mode pattern is determined by the formula $m_R = nB + KV$, where n is the harmonic number, K is an integer ($K = \dots -1, 0, 1, 2 \dots$), and V is the number of stator vanes. If a particular pattern has fewer lobes than rotor blades, it rotates faster than the rotor shaft in order to generate the same frequency. If the pattern has more lobes, it rotates slower.

Thus, it is seen that the circumferential Mach number of each of the various lobe patterns is dependent not only on the rotor speed, as in the case of the rotor alone, but also on the number of rotor blades and the number of stationary vanes in the proximity of the rotor. The sign of m can be either positive or negative, depending on its rotational direction. A positive sign means the lobe pattern is rotating in the same direction as the rotor and a negative sign means it is rotating in the opposite direction. The lobe pattern of interest for each harmonic number n is the one having the lowest value of m .

Both upstream and downstream stationary vanes in the proximity of the rotor may interact with the rotor to generate additional lobe patterns, each rotating at the same frequency as the rotor blade-passage frequency. If the circumferential Mach number of any lobe pattern is supersonic, it is said to be above "cut-off" and the pressure field propagates freely along the duct; however, if the circumferential Mach number of the spinning

mode is subsonic, the pressure field decays. (See ref. 4.) The modes which propagate freely in an axial-flow compressor are thus of primary concern in evaluating the far-field noise.

Table I gives calculated values of m_R for the first two stages of the compressor used in this study. The numbers of lobes tabulated in table I(a) are based on the IGV or upstream stator ($V_0 = 41$) interactions with the first-stage rotor, the numbers of lobes in table I(b) are based on the first-stage stator ($V_1 = 36$) interactions with the first-stage rotor, and the numbers of lobes in table I(c) are based on the first-stage stator ($V_1 = 36$) interactions with the second-stage rotor. The interactions between the upstream stator and the rotor generally predominate and thus, in most cases, only these interactions are considered. When the spinning modes associated with the upstream stator are below cut-off and those associated with the downstream stator are above cut-off, interactions between the rotor and the downstream stator may predominate.

The cut-off ratios or predictions of propagation of the spinning-mode patterns of table I are given in table II for the three test rotor speeds, 4830 rpm (35 percent), 8280 rpm (60 percent), and 11 040 rpm (80 percent). For values of cut-off ratio ξ greater than unity, propagation along the duct is predicted. On the other hand, for values below unity, decay is predicted and the rate of decay increases with decreasing cut-off ratio ξ . It can be seen from table II that all the modes for the higher speeds are expected to propagate, whereas two of the modes for the speed of 35-percent rpm (for the IGV interactions with the first-stage rotor) are expected to decay. The effect of the cut-off ratio presented in table II is confirmed by the data of figures 8 and 9. The fact that the circumferential Mach number of the spinning mode for the first-stage-rotor fundamental frequency ($n = 1$) is only slightly above unity for the 8280-rpm condition ($\xi = 1.09$ from table II(a)) may explain why the relative amplitude of the peak corresponding to this frequency is less than that of the peak corresponding to the frequency of the second-stage rotor ($\xi = 2.63$ from table II(c)), as shown in figure 8 for the condition of 60-percent rpm. The measurements obtained at 35-percent rated rpm (4830 rpm) and presented in figure 9 clearly demonstrate the analytical predictions of table II(a) regarding the cut-off concept. Figure 9 shows a spectrum of the noise at 35-percent rpm for the standard engine, as obtained with a 50-hertz constant-bandwidth filter. The various peaks associated with the rotor are identified in the figure, where it can be seen that neither the first nor second harmonic of the first-stage rotor is identifiable. This would be expected on the basis of the calculations of table II(a), which indicate that neither of these modes should propagate in the duct. Apparently the interactions of the first rotor with the first stator (table II(b)), although the modes produced are above cut-off, are of minor importance.

Noise generation by stators.- An examination of the spectra in figures 8 and 9 shows that some of the peaks are not identifiable with either the rotors or their harmonic frequencies. These peaks are apparently associated with the stator vanes, which can be

sources of noise when impinged upon by pulsating flows, as would be present on the discharge side of a rotor. In the coordinate system which rotates with the rotor, the frequencies associated with such flow impingements are determined by the product of the flow rotational speed (equal to the rotor speed) and the number of stator vanes. The validity of the rotating-coordinate-system assumption is supported by the frequency-spectra data of figures 8 and 9, in which many of the otherwise unidentifiable peaks are associated with the stators. In addition, these stator-generated spinning modes are noted to conform to the same cut-off concepts as the rotor-generated modes of reference 4.

Based on the above concept of rotating coordinates, the following relation applies to the determination of lobe patterns for the associated stator-generated spinning modes: $m_S = nV + KB$, where the quantities involved are the same as previously used in the determination of the number of lobes of the rotor-generated spinning modes m_R . The above relationship has been used to calculate the values of m_S in table III.

Table III gives calculated values of m_S for the IGV and first two stator stages based on the assumption that the pulsating flow field is rotating at the same speed as the rotor. The cut-off ratios ξ associated with the spinning-mode patterns of table III are given in table IV for the IGV and the first- and second-stage stators at the three test compressor speeds.

At a 4830-rpm speed, the lobe patterns from the fundamental and second harmonic of the first-stage rotor interacting with the IGV do not propagate (table II(a)); however, the lobe patterns of the first-stage stator do propagate (table IV(b)). At this rotor speed, the spectrum for the 30° azimuth angle for the standard engine (fig. 9) shows the noise peaks at frequencies associated with both the IGV and first-stage stator to be higher than the peaks associated with the first-stage rotor. This result may be expected in view of the cut-off phenomena for the lobe patterns, as shown in tables II(a) and IV.

It can be seen from tables II(a) and IV that at the 60-percent and 80-percent speeds, propagation of both the rotor-generated and stator-generated modes is expected. Figures 6 and 8 (for speeds of 80-percent rpm and 60-percent rpm, respectively) indicate that although both rotor-generated and stator-generated noise is expected to propagate, the noise from the rotor predominates. When the lobe patterns from the rotor are below cut-off and those from the stator are above cut-off, the lobe pattern from the stator may predominate.

In addition to examining the narrow-band frequency analysis of the standard engine at various speeds, it is also of interest to examine similar data for the modified engine (increased IGV-rotor spacing). The result of this analysis is shown in figure 10. This figure shows spectra of the noise at all three test speeds, as obtained with a 50-hertz constant-bandwidth filter. The spectra for the standard engine (shown by the solid curves)

are repeated for comparison, the data for the speeds of 35-percent rpm and 60-percent rpm being the same as the data presented in figures 9 and 8, respectively.

The data for the modified engine (dashed curves) show large noise reductions from the noise level of the standard engine for all speeds. Of particular interest is the large reduction (8 to 10 dB) in the broadband level over the entire range of frequencies, a reduction not found for the model tested in references 1 and 2. This reduction, however, is in line with the results of reference 5, where it is shown that small increases in IGV-rotor spacing (on the order of one-half chord) are sufficient to realize substantial reductions in broadband noise due to the wake turbulence. This reference also indicated that further increases in spacing give small additional reduction in this type of noise. The minimum IGV-rotor spacing used in the investigations of both references 1 and 2 is one-half chord so that the major reductions in the broadband noise have already been realized. In the present investigation, however, the minimum spacing is one-eighth chord so that increased spacing would be expected to result in substantial reductions in the broadband noise.

Furthermore, the discrete tones have been greatly reduced, which is in agreement with the results in references 1 and 2. It is also noted that, in general, the noise peaks corresponding to the second-stage-rotor frequencies and the peaks corresponding to the stator frequencies are greatly reduced or almost eliminated with increased spacing. A notable exception occurs for the speed of 35-percent rpm, where the modified-engine curve has peaks not shown for the standard engine, for example, at 2335 hertz, corresponding to B_1N . This spinning mode is below cut-off when based on the rotor and upstream stator (table II(a)), but is above cut-off when based on the rotor and downstream stator (table II(b)).

It should be noted that there are several distinct noise peaks in the spectra of figure 10 which do not correspond to either the rotor or stator frequencies. Analyses indicate that these peaks occur at combinations of tones, that is, at sums or differences of frequencies of adjacent components of the compressor. The phenomena of generation of these combination tones have been noted by other investigators and are discussed in reference 6.

CONCLUSIONS

Studies of a turbojet engine in the 2000-pound (8896-newton) thrust category, in which performance and noise measurements were made, indicate the following conclusions:

1. Noise reductions due to increased inlet-guide-vane—rotor spacing have been accomplished without any measurable loss in engine performance.

2. Increased inlet-guide-vane—rotor spacing resulted in substantial reductions in the overall noise level over the entire front quadrant for all test engine speeds. The reductions were as much as 14 dB for the condition of 80-percent rated rpm, the highest engine speed at which noise measurements were made.

3. Increased inlet-guide-vane—rotor spacing resulted in large reductions in the broadband noise as well as in the noise levels at the fundamental blade-passage frequency and almost eliminated the higher harmonics of the blade-passage frequency.

4. Stationary components of the compressor which are exposed to pulsating flows are identified as sources of noise and are noted to have characteristic frequencies.

Langley Research Center,
National Aeronautics and Space Administration,
Langley Station, Hampton, Va., April 29, 1968,
126-61-03-01-23.

REFERENCES

1. Crigler, John L.; and Copeland, W. Latham: Noise Studies of Inlet-Guide-Vane—Rotor Interaction of a Single-Stage Axial-Flow Compressor. NASA TN D-2962, 1965.
2. Copeland, W. Latham; Crigler, John L.; and Dibble, Andrew C., Jr.: Contribution of Downstream Stator to the Interaction Noise of a Single-Stage Axial-Flow Compressor. NASA TN D-3892, 1967.
3. Anon.: Measurements of Aircraft Exterior Noise in the Field. ARP 796, Soc. Automotive Eng., June 15, 1965.
4. Tyler, J. M.; and Sofrin, T. G.: Axial Flow Compressor Noise Studies. SAE Trans., vol. 70, 1962, pp. 309-332.
5. Sharland, I. J.: Sources of Noise in Axial Flow Fans. J. Sound Vib., vol. 1, no. 3, July 1964, pp. 302-322.
6. Kinsler, Lawrence E.; and Frey, Austin R.: Fundamentals of Acoustics. Second ed., John Wiley & Sons, Inc., c.1962, pp. 402-406.

TABLE I.- NUMBER OF LOBES FOR COMPRESSOR ROTOR CONFIGURATIONS

(a) First-stage rotor. $B_1 = 29$; $V_0 = 41$.

K	m_R		
	n = 1	n = 2	n = 3
-3	-94	-65	-36
-2	-53	-24	5
-1	-12	17	46
0	29	58	87
1	70	99	128

(b) First-stage rotor. $B_1 = 29$; $V_1 = 36$.

K	m_R		
	n = 1	n = 2	n = 3
-3	-79	-50	-21
-2	-43	-14	15
-1	-7	22	51
0	29	58	87

(c) Second-stage rotor. $B_2 = 43$; $V_1 = 36$.

K	m_R		
	n = 1	n = 2	n = 3
-3	-65	-22	21
-2	-29	14	57
-1	7	50	93
0	43	86	129

TABLE II.- PREDICTION OR PROPAGATION FOR ROTORS

(a) First-stage rotor. $B_1 = 29$; $V_0 = 41$.

N, rpm	M_t	m_R	n	$K'_{m\mu}$	f, Hz	ξ	Propagate
11 040	0.705	12	1	14.0	5 335	1.46	Yes
11 040	.705	17	2	19.0	10 670	2.15	Yes
11 040	.705	5	3	6.15	16 005	9.98	Yes
8 280	.529	12	1	14.0	4 000	1.09	Yes
8 280	.529	17	2	19.0	8 000	1.62	Yes
8 280	.529	5	3	6.15	12 000	7.48	Yes
4 830	.3085	12	1	14.0	2 335	.638	No
4 830	.3085	17	2	19.0	4 670	.942	No
4 830	.3085	5	3	6.15	7 005	4.36	Yes

(b) First-stage rotor. $B_1 = 29$; $V_1 = 36$.

N, rpm	M_t	m_R	n	$K'_{m\mu}$	f, Hz	ξ	Propagate
11 040	0.705	7	1	8.65	5 335	2.36	Yes
11 040	.705	14	2	16.0	10 670	2.56	Yes
11 040	.705	15	3	16.95	16 005	3.62	Yes
8 280	.529	7	1	8.65	4 000	1.77	Yes
8 280	.529	14	2	16.00	8 000	1.92	Yes
8 280	.529	15	3	16.95	12 000	2.98	Yes
4 830	.3085	7	1	8.65	2 335	1.03	Yes
4 830	.3085	14	2	16.0	4 670	1.12	Yes
4 830	.3085	15	3	16.95	7 005	1.58	Yes

(c) Second-stage rotor. $B_2 = 43$; $V_1 = 36$.

N, rpm	M_t	m_R	n	$K'_{m\mu}$	f, Hz	ξ	Propagate
11 040	0.705	7	1	8.65	7 910	3.50	Yes
11 040	.705	14	2	16.0	15 820	3.79	Yes
8 280	.529	7	1	8.65	5 930	2.63	Yes
8 280	.529	14	2	16.0	11 860	2.84	Yes
4 830	.3085	7	1	8.65	3 460	1.53	Yes
4 830	.3085	14	2	16.0	6 920	1.66	Yes
4 830	.3085	21	3	23.2	10 380	1.72	Yes

TABLE III.- NUMBER OF LOBES FOR COMPRESSOR IGV
AND STATOR CONFIGURATIONS

(a) IGV. $V_0 = 41$; $B_1 = 29$.

K	m _S		
	n = 1	n = 2	n = 3
-4	-75	-34	7
-3	-46	-5	36
-2	-17	24	65
-1	12	53	94
0	41	82	123

(b) First-stage stator. $V_1 = 36$; $B_1 = 29$.

K	m _S		
	n = 1	n = 2	n = 3
-3	-51	-15	21
-2	-22	14	50
-1	7	43	79
0	36	72	108

(c) Second-stage stator. $V_2 = 48$; $B_2 = 43$.

K	m _S		
	n = 1	n = 2	n = 3
-3	-81	-33	15
-2	-38	10	58
-1	5	53	101

TABLE IV.- PREDICTION OF PROPAGATION FOR IGV AND STATORS

(a) IGV. $V_0 = 41$; $B_1 = 29$.

N, rpm	mg	n	$K'_{m\mu}$	f, Hz	ξ	Propagate
11 040	12	1	14.0	7 540	2.06	Yes
11 040	5	2	6.15	15 080	9.40	Yes
8 280	12	1	14.0	5 660	1.55	Yes
8 280	5	2	6.15	11 320	7.06	Yes
4 830	12	1	14.0	3 300	.90	No
4 830	5	2	6.15	6 600	4.11	Yes
4 830	7	3	8.65	9 900	4.39	Yes

(b) First-stage stator. $V_1 = 36$; $B_1 = 29$.

N, rpm	mg	n	$K'_{m\mu}$	f, Hz	ξ	Propagate
11 040	7	1	8.65	6 620	2.97	Yes
11 040	14	2	16.0	13 240	3.22	Yes
8 280	7	1	8.65	4 970	2.20	Yes
8 280	14	2	16.0	9 940	2.38	Yes
4 830	7	1	8.65	2 900	1.28	Yes
4 830	14	2	16.0	5 800	1.39	Yes
4 830	21	3	23.2	8 700	1.44	Yes

(c) Second-stage stator. $V_2 = 48$; $B_2 = 43$.

N, rpm	mg	n	$K'_{m\mu}$	f, Hz	ξ	Propagate
11 040	5	1	6.15	8 830	5.50	Yes
11 040	10	2	12.0	17 660	5.64	Yes
8 280	5	1	6.15	6 625	4.13	Yes
8 280	10	2	12.0	13 250	4.23	Yes
4 830	5	1	6.15	3 865	2.41	Yes
4 830	10	2	12.0	7 730	2.47	Yes
4 830	15	3	16.95	11 595	2.62	Yes

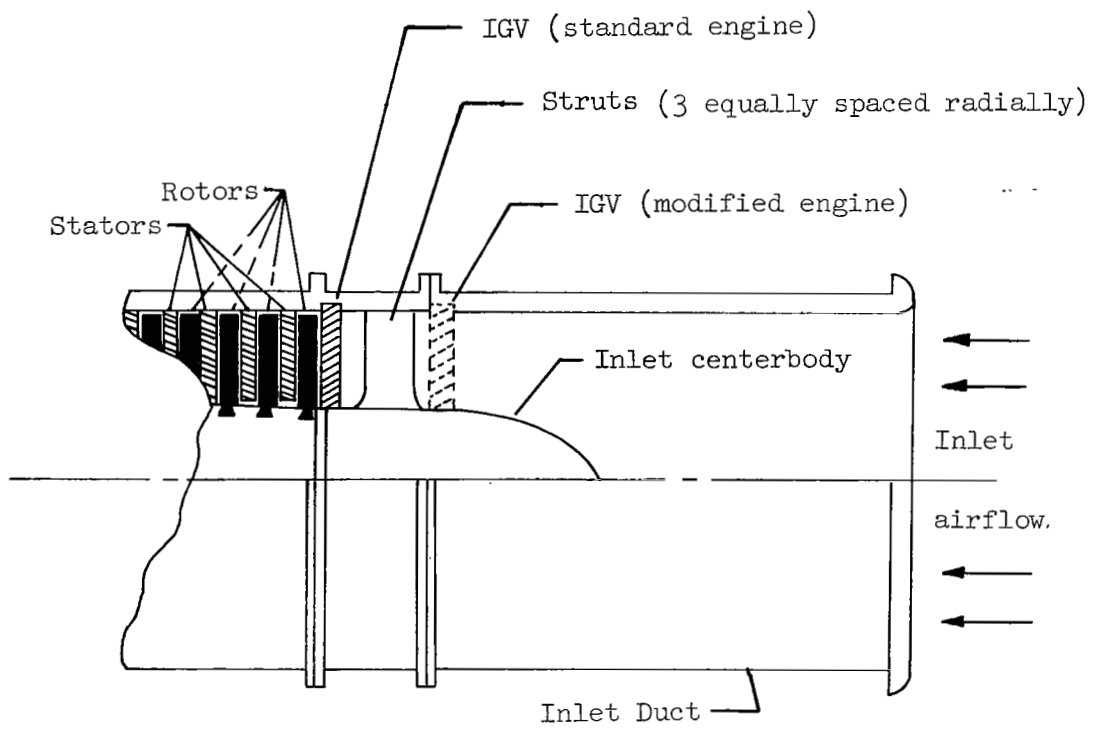


Figure 1.- Cross-section sketch of inlet showing the relative locations of rotating and stationary components for the standard and modified engine.

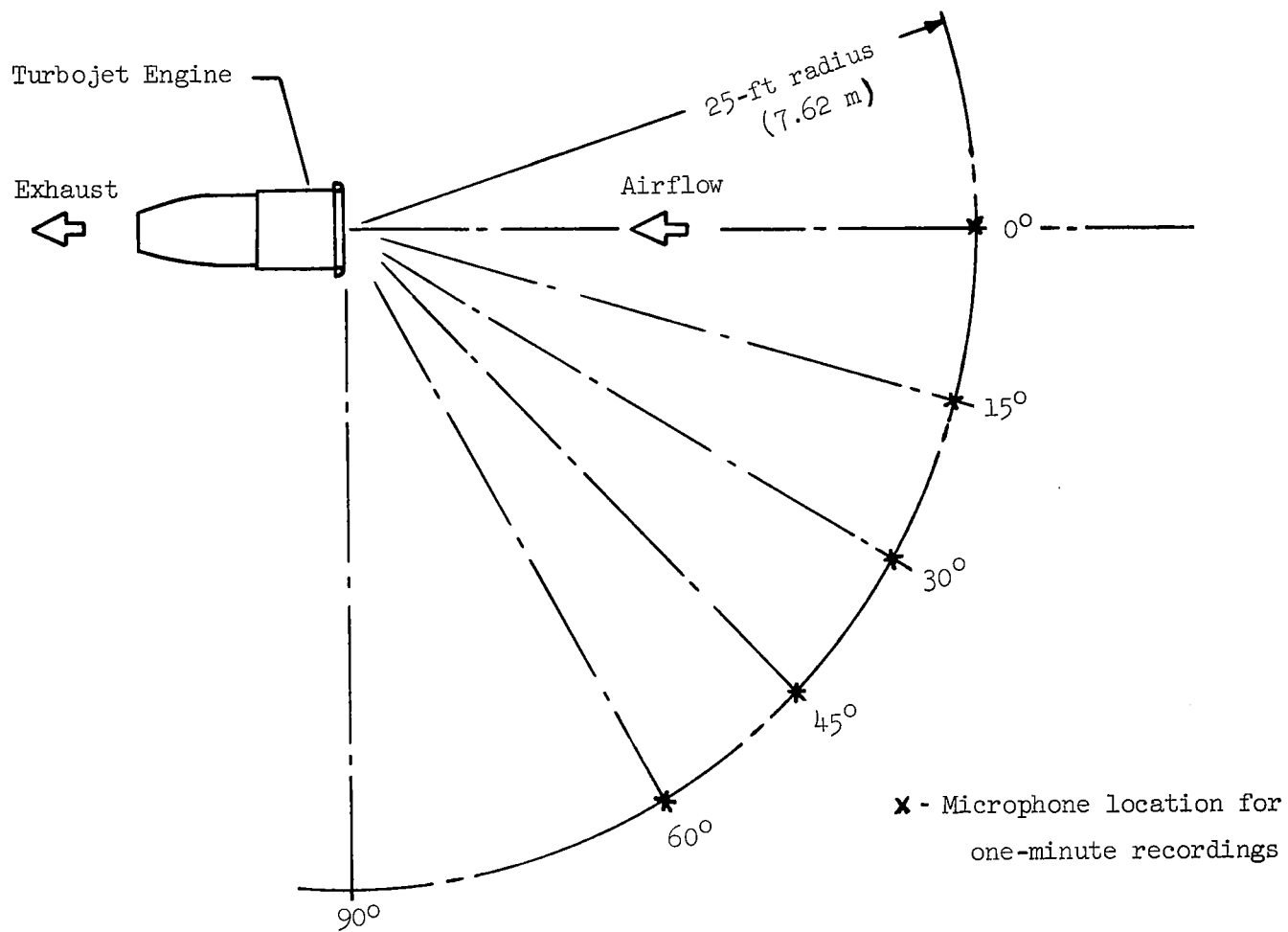
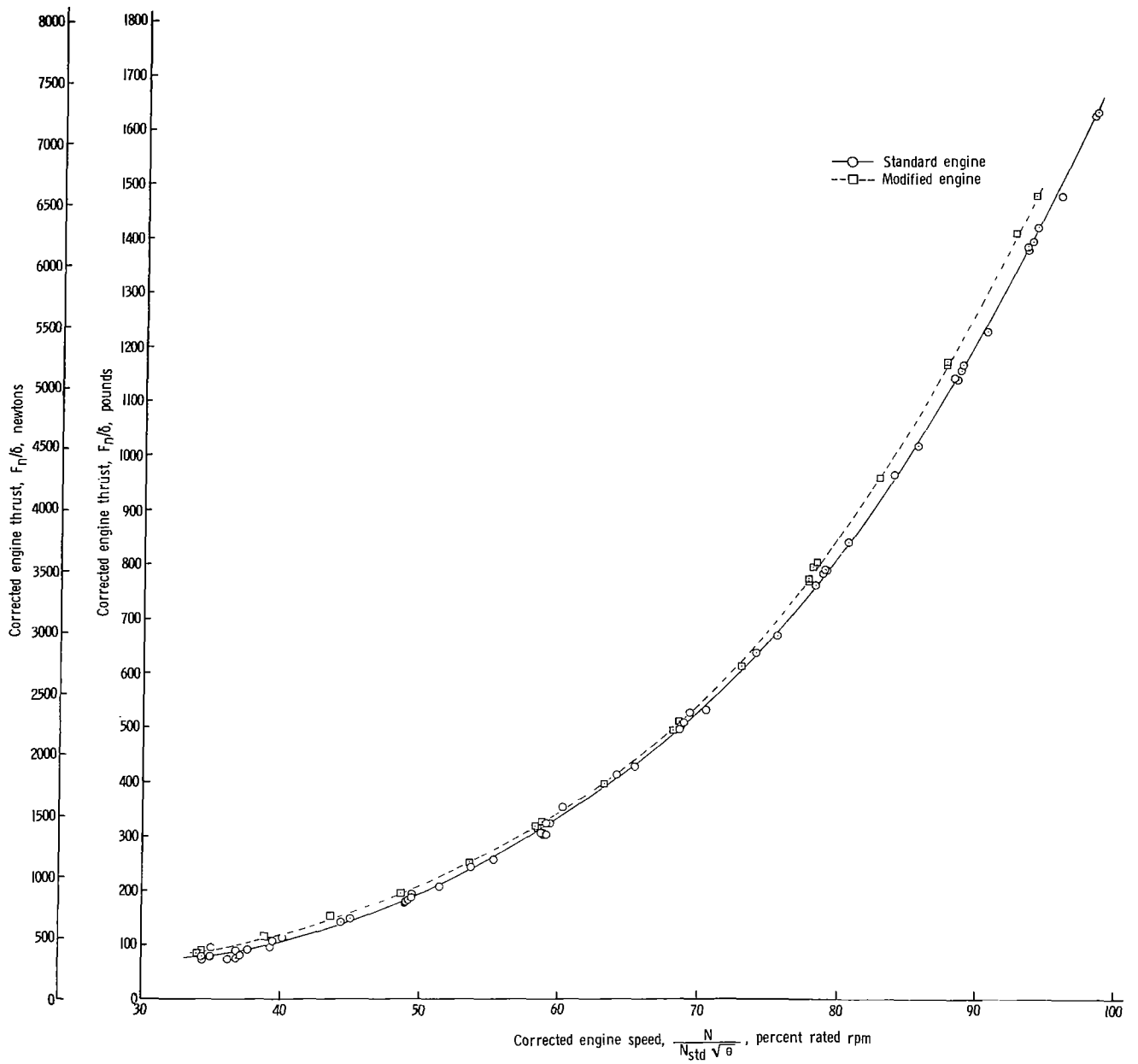
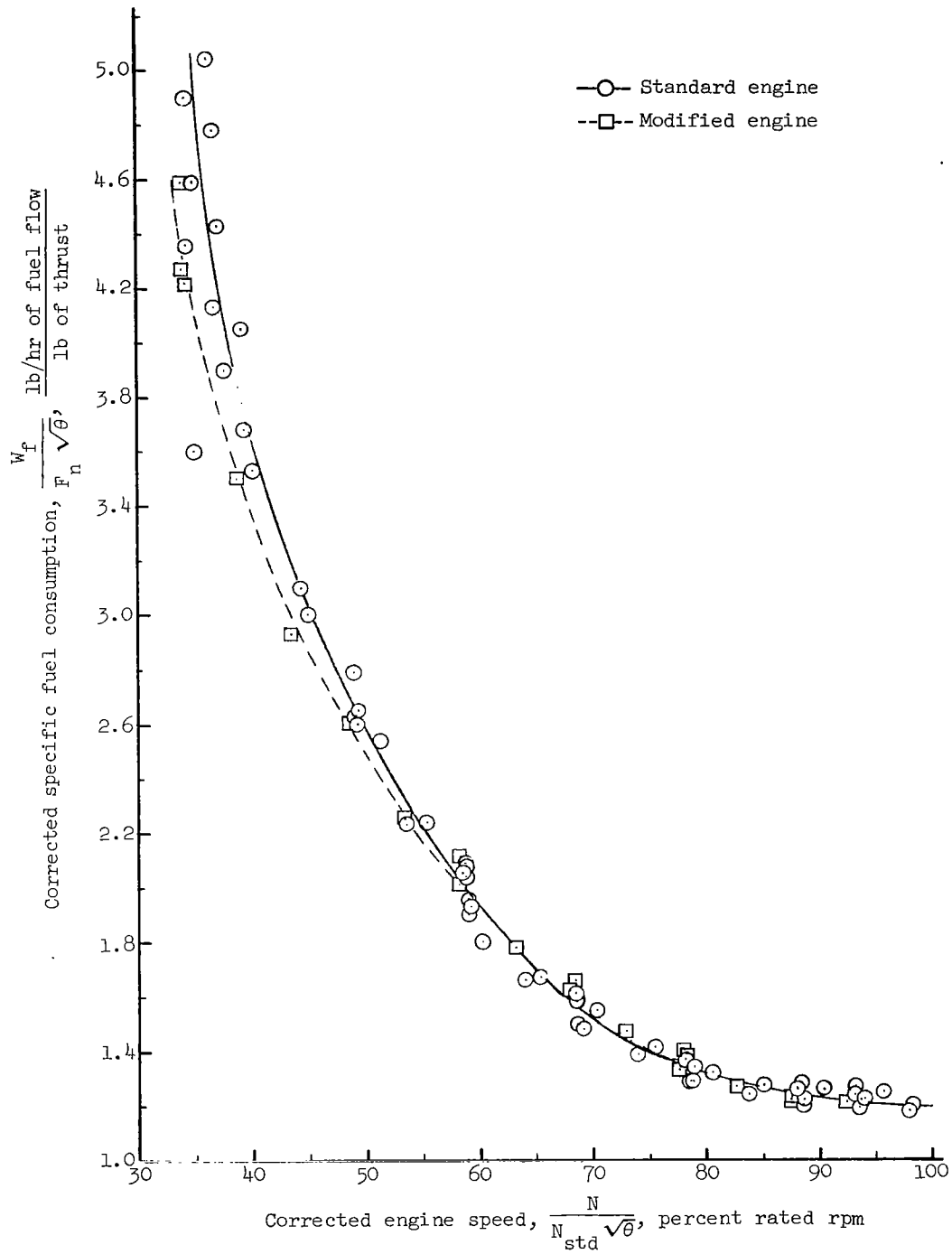


Figure 2.- Plan-view sketch of test area showing turbojet engine and noise-measuring locations.



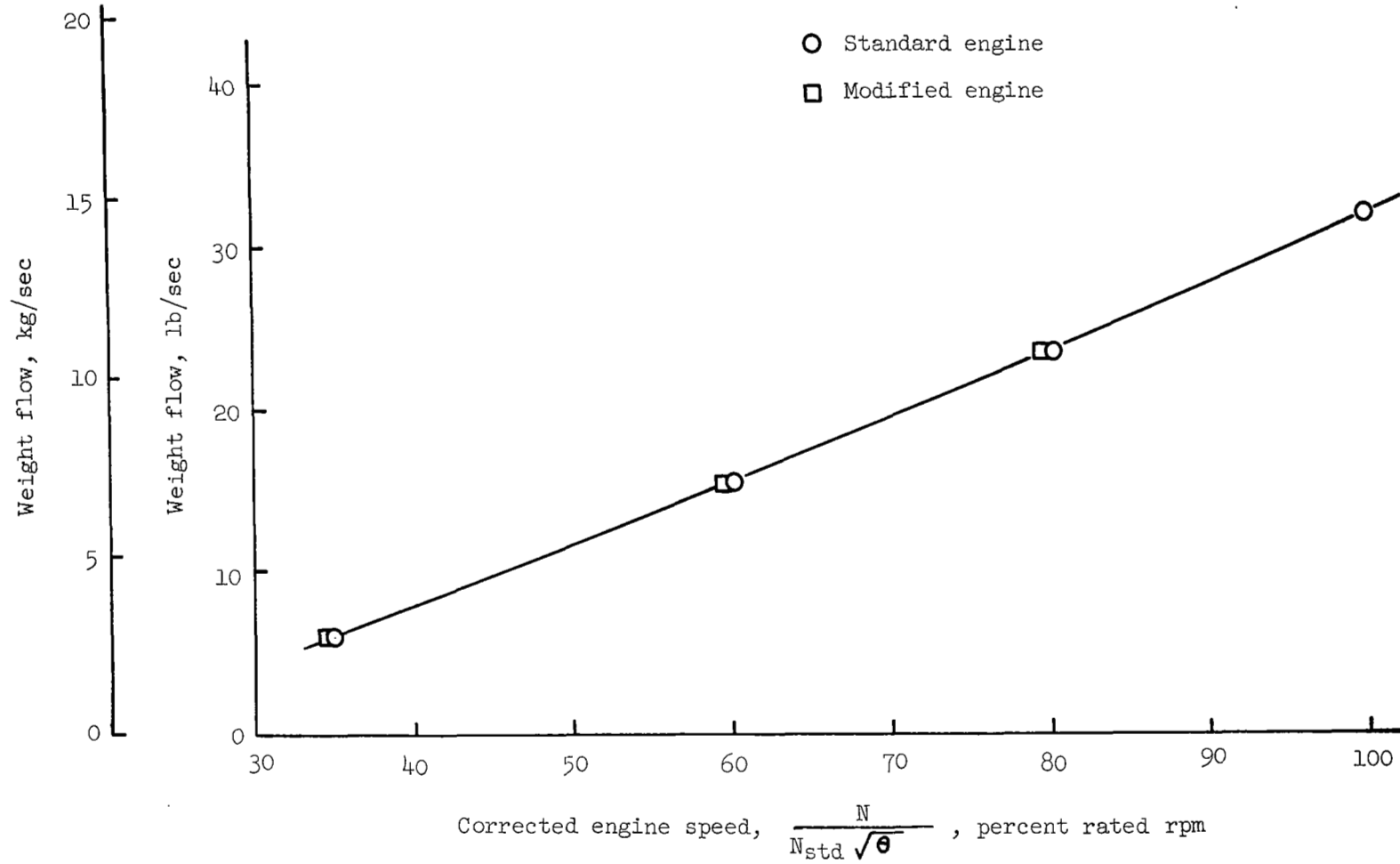
(a) Thrust.

Figure 3.- Variation of performance with engine speed for standard and modified engine.



(b) Specific fuel consumption.

Figure 3.- Continued.



(c) Airflow.

Figure 3.- Concluded.

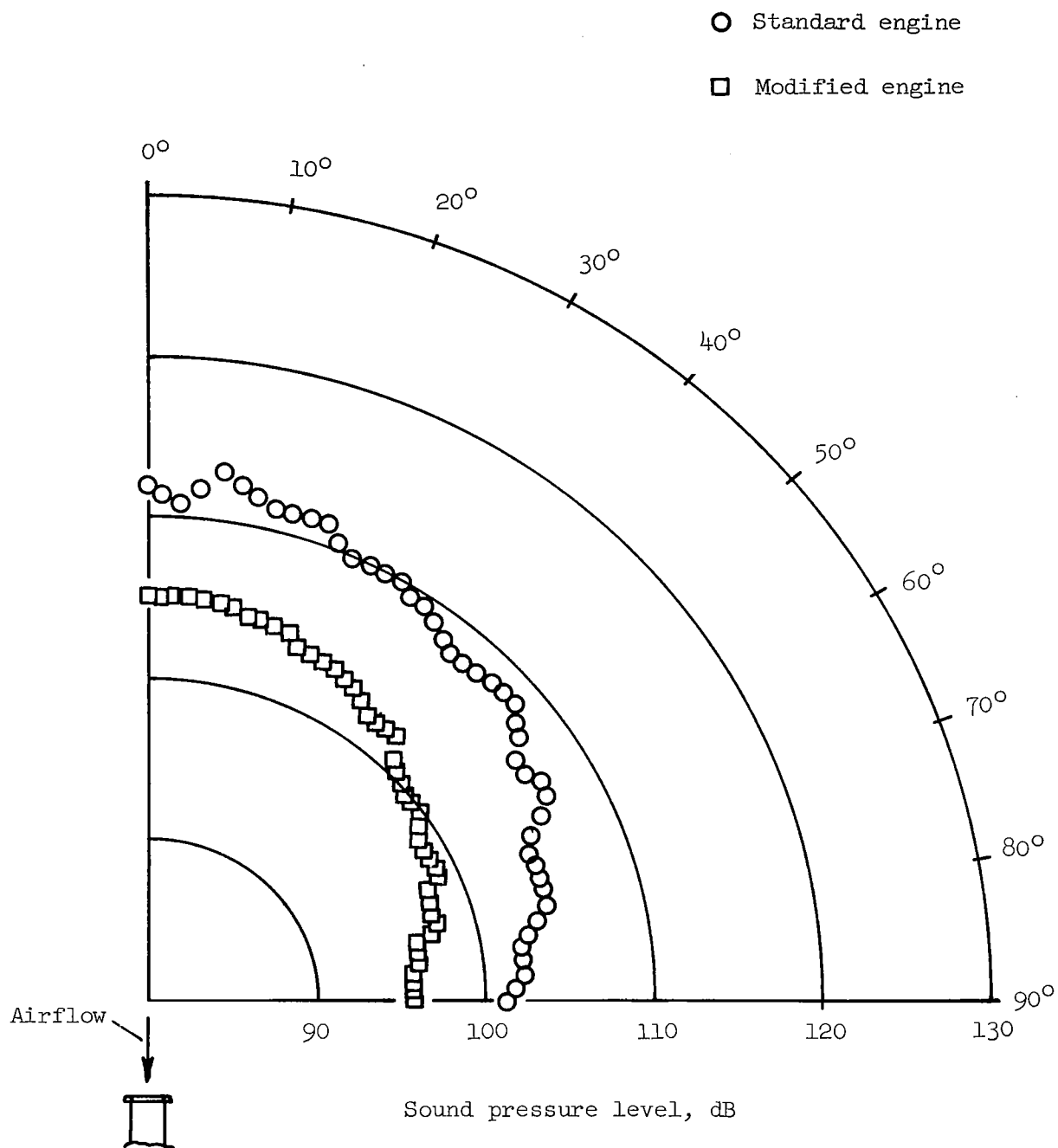
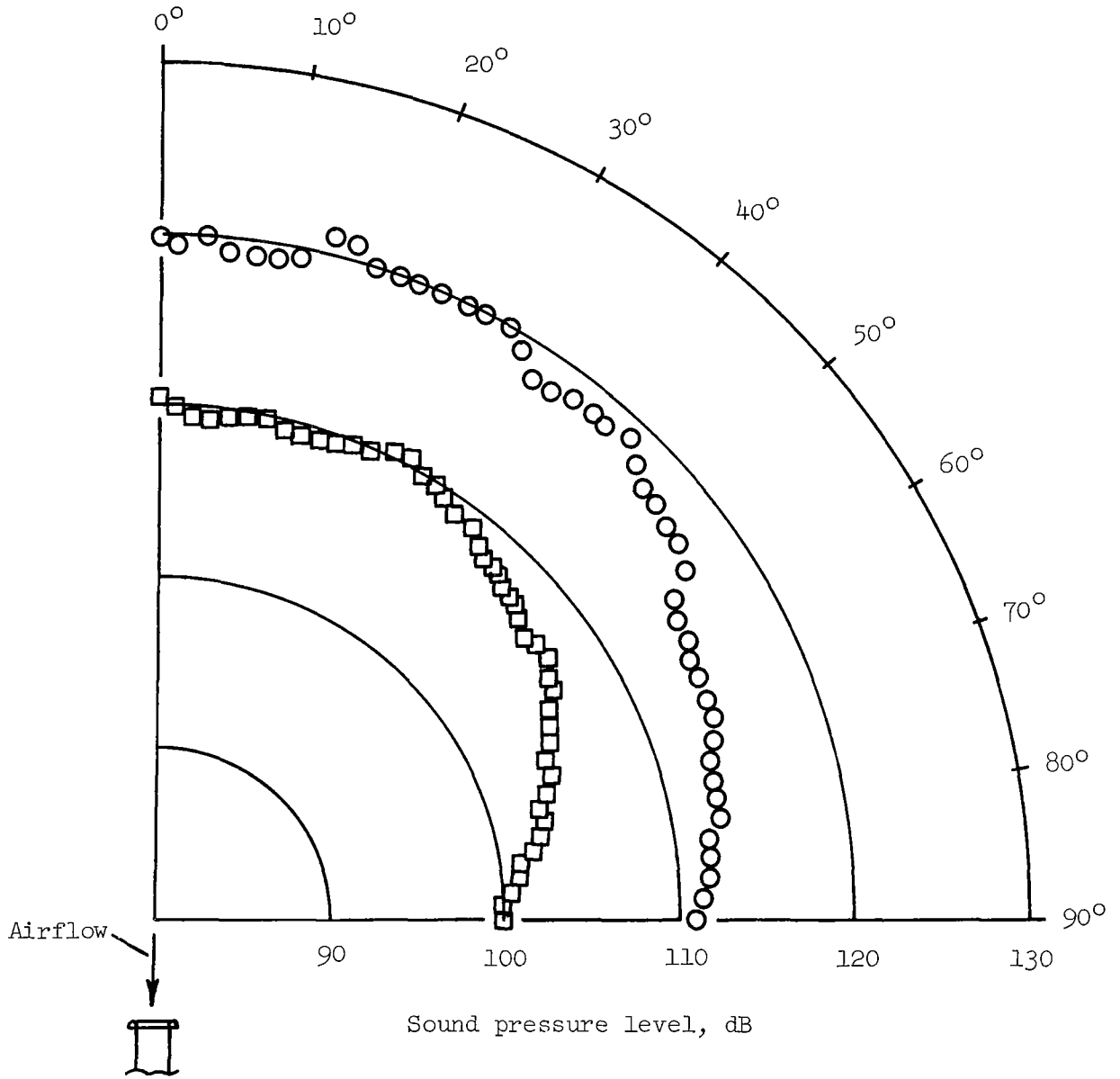


Figure 4.- Overall radiation patterns for standard and modified engine as a function of azimuth angle for three engine speeds as measured on a 25-foot (7.62-meter) radius.

- Standard engine
- Modified engine

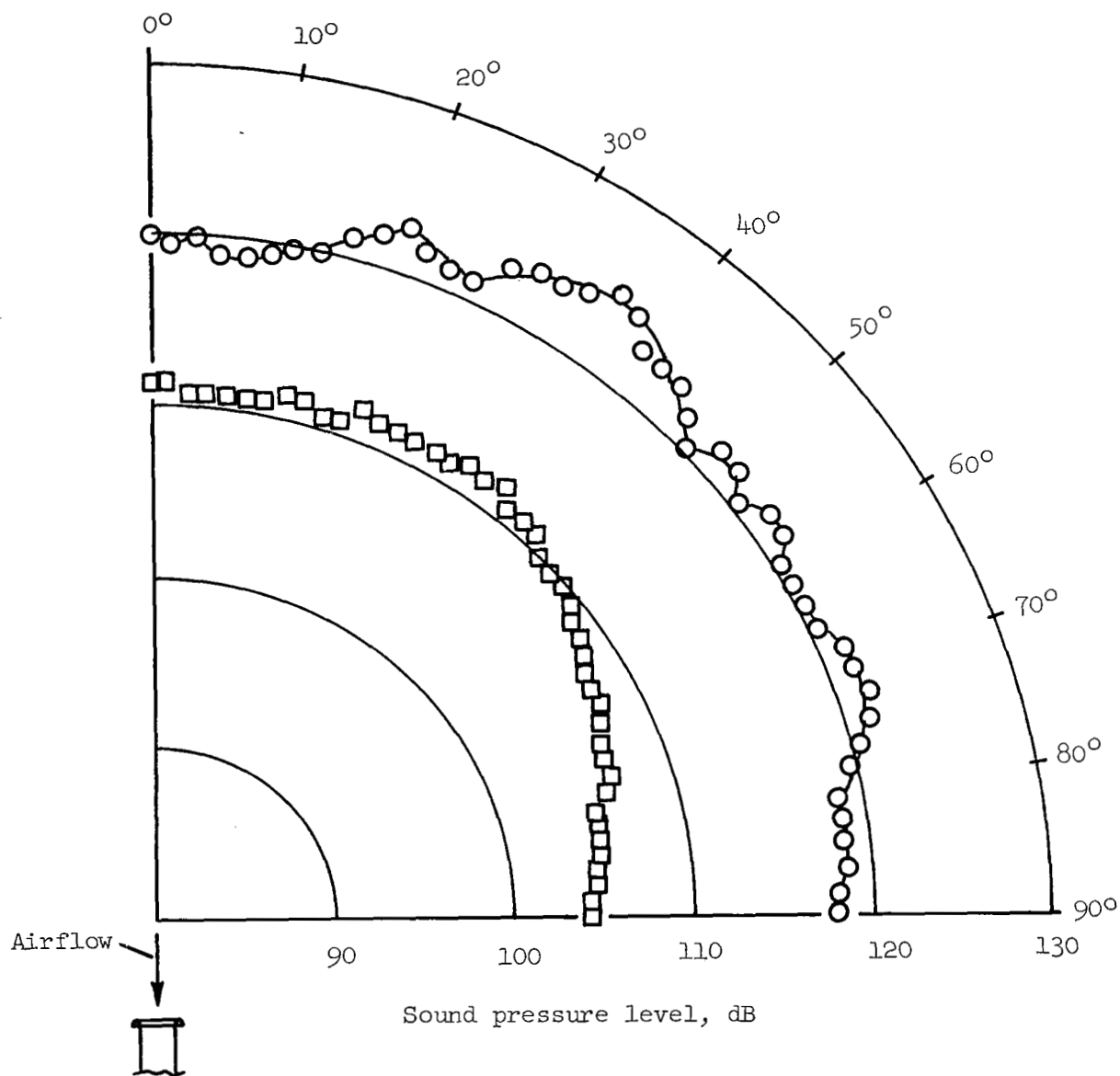


(b) 60-percent rpm.

Figure 4.- Continued.

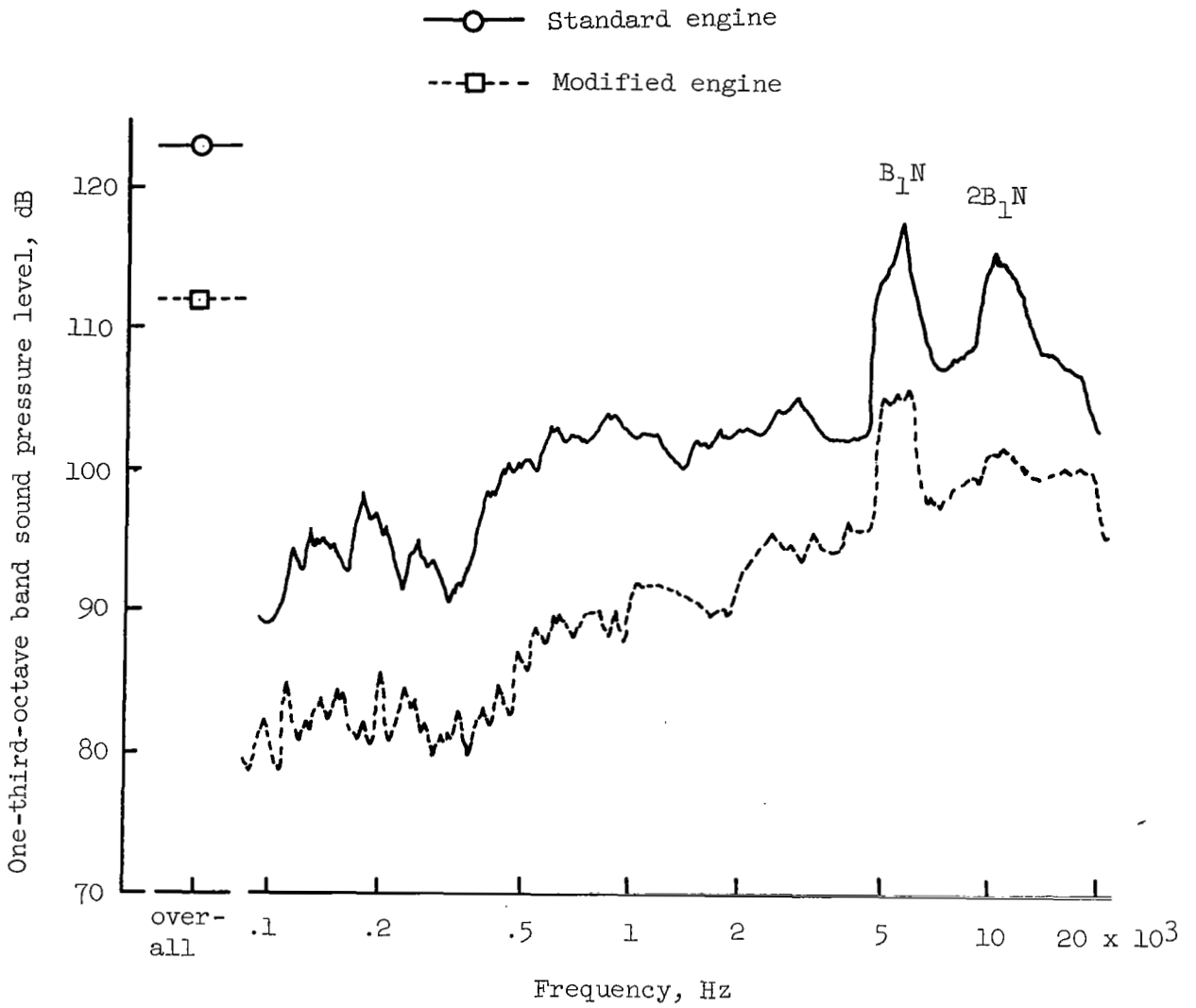
○ Standard engine

□ Modified engine



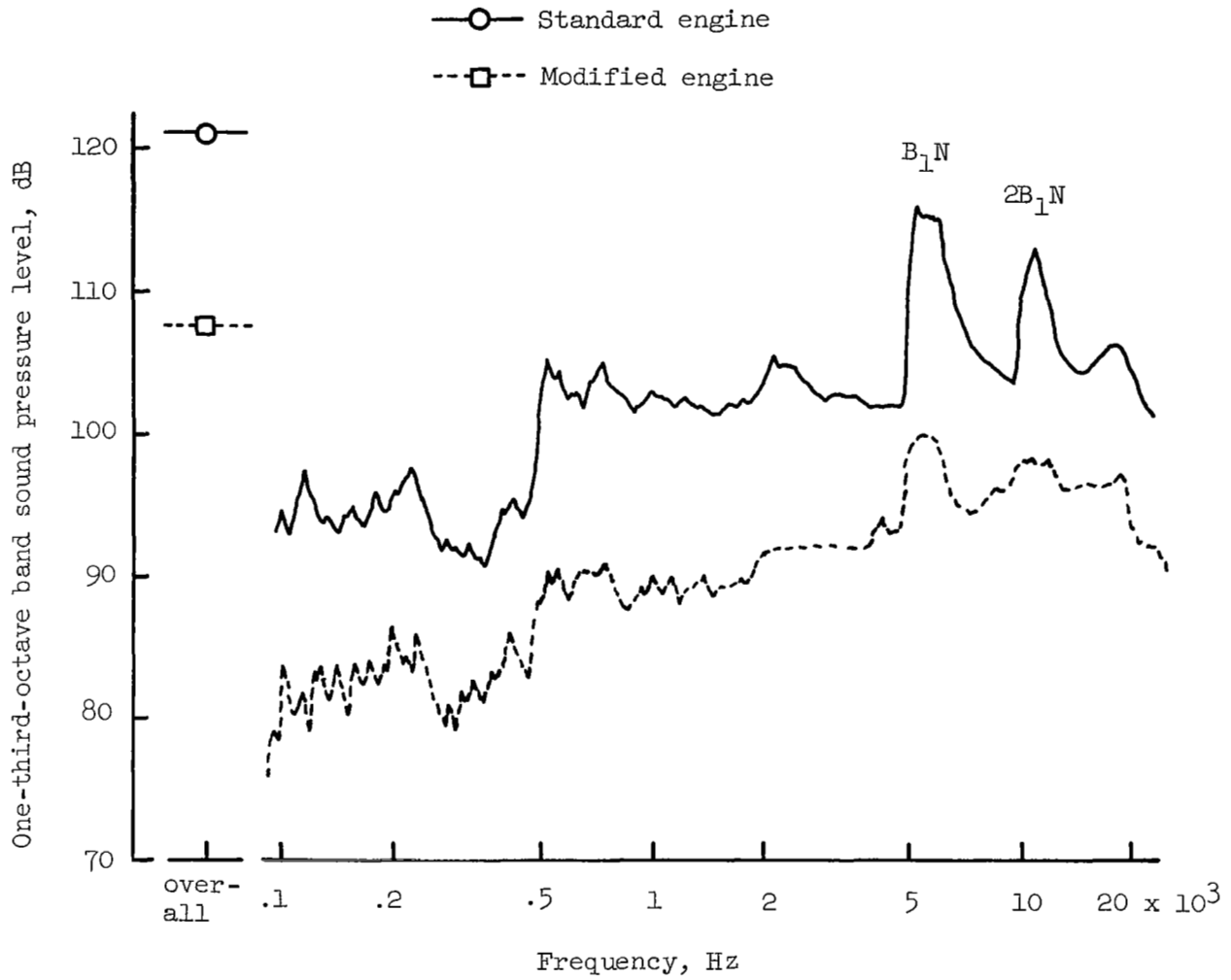
(c) 80-percent rpm.

Figure 4.- Concluded.



(a) 30° azimuth.

Figure 5.- One-third-octave band frequency spectra for standard and modified engine for two azimuth locations as measured on a 25-foot (7.62-meter) radius for an engine speed of 80-percent rated rpm.



(b) 60° azimuth.

Figure 5.- Concluded.

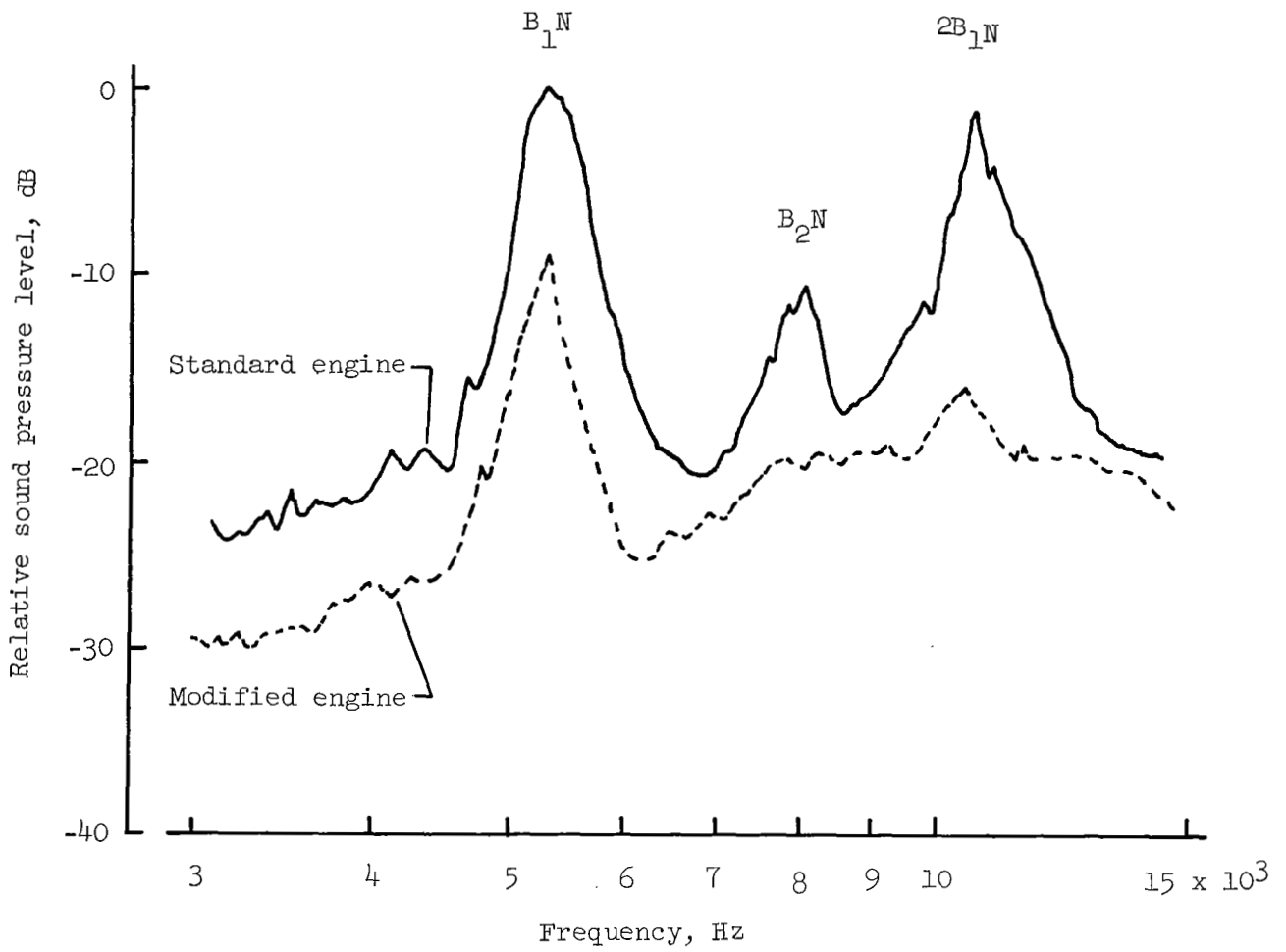


Figure 6.- One-tenth-octave band frequency analysis for standard and modified engine for 30° azimuth location as measured on a 25-foot (7.62-meter) radius for an engine speed of 80-percent rated rpm.

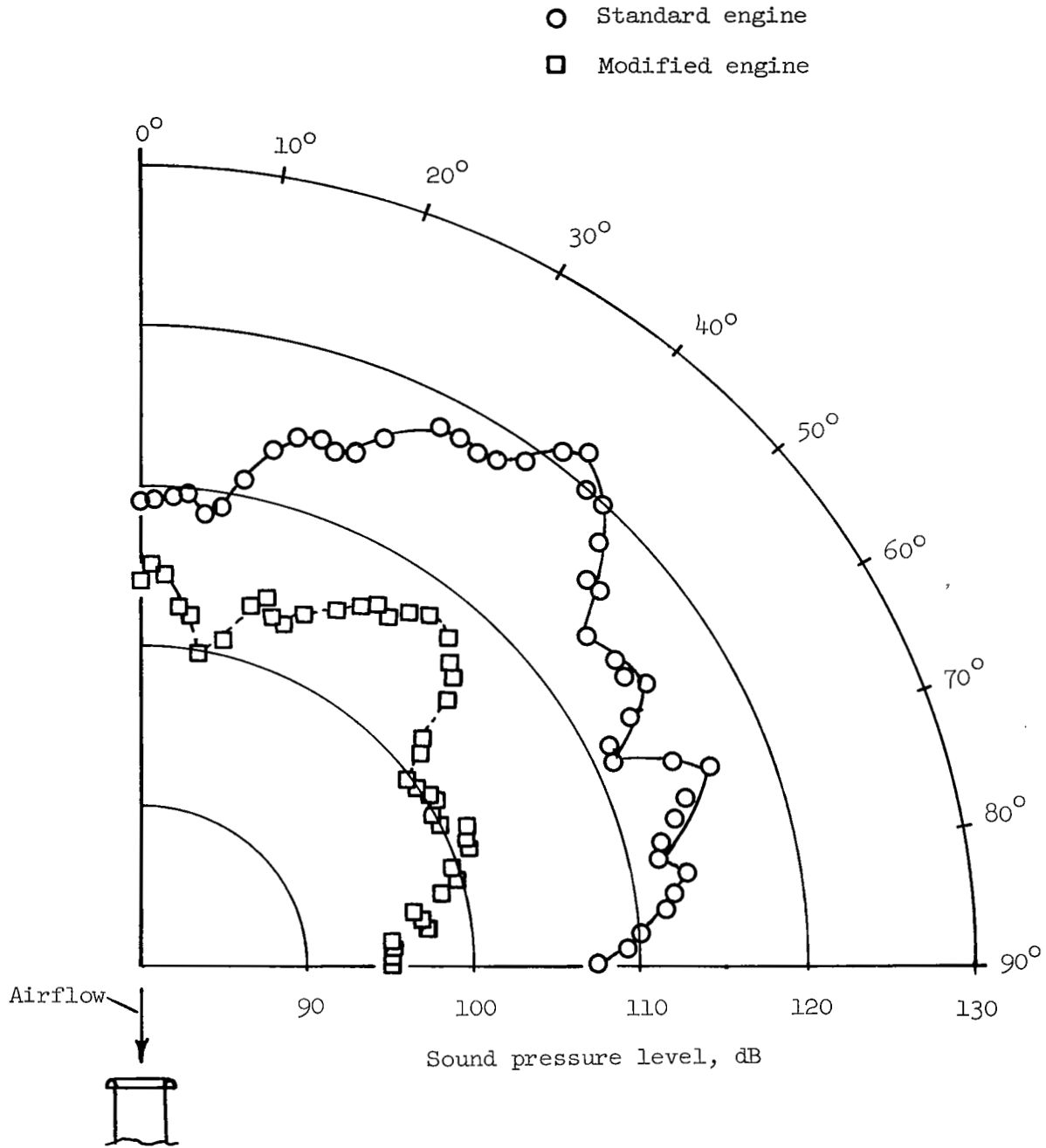


Figure 7.- One-third-octave band (centered at first-stage-rotor fundamental blade frequency) radiation patterns for standard and modified engine as a function of azimuth angle as measured on a 25-foot (7.62-meter) radius for an engine speed of 80-percent rated rpm.

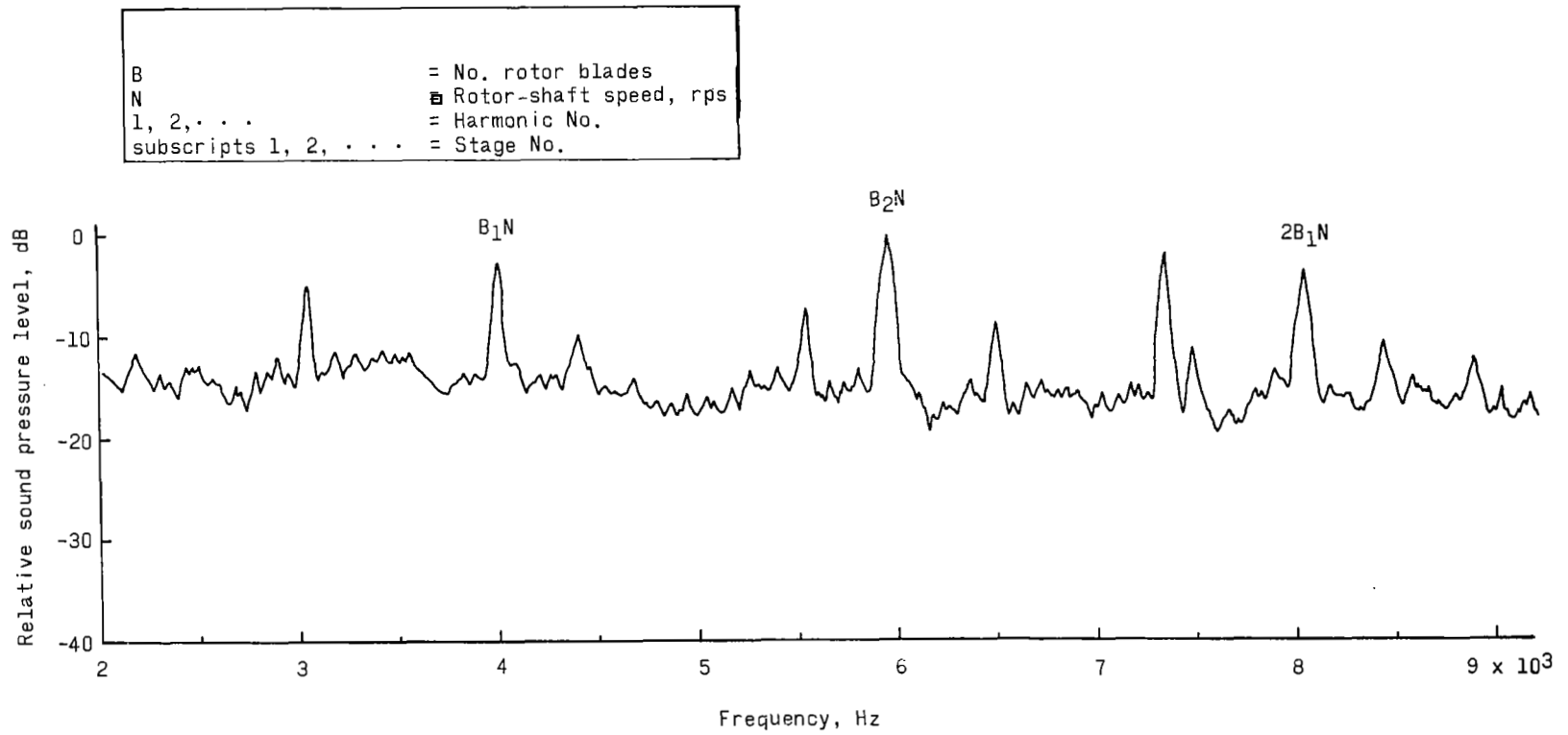


Figure 8.- Frequency analysis, using 50-hertz constant-bandwidth filter, for standard engine as measured at 30^o azimuth location on a 25-foot (7.62-meter) radius for an engine speed of 60-percent rated rpm.

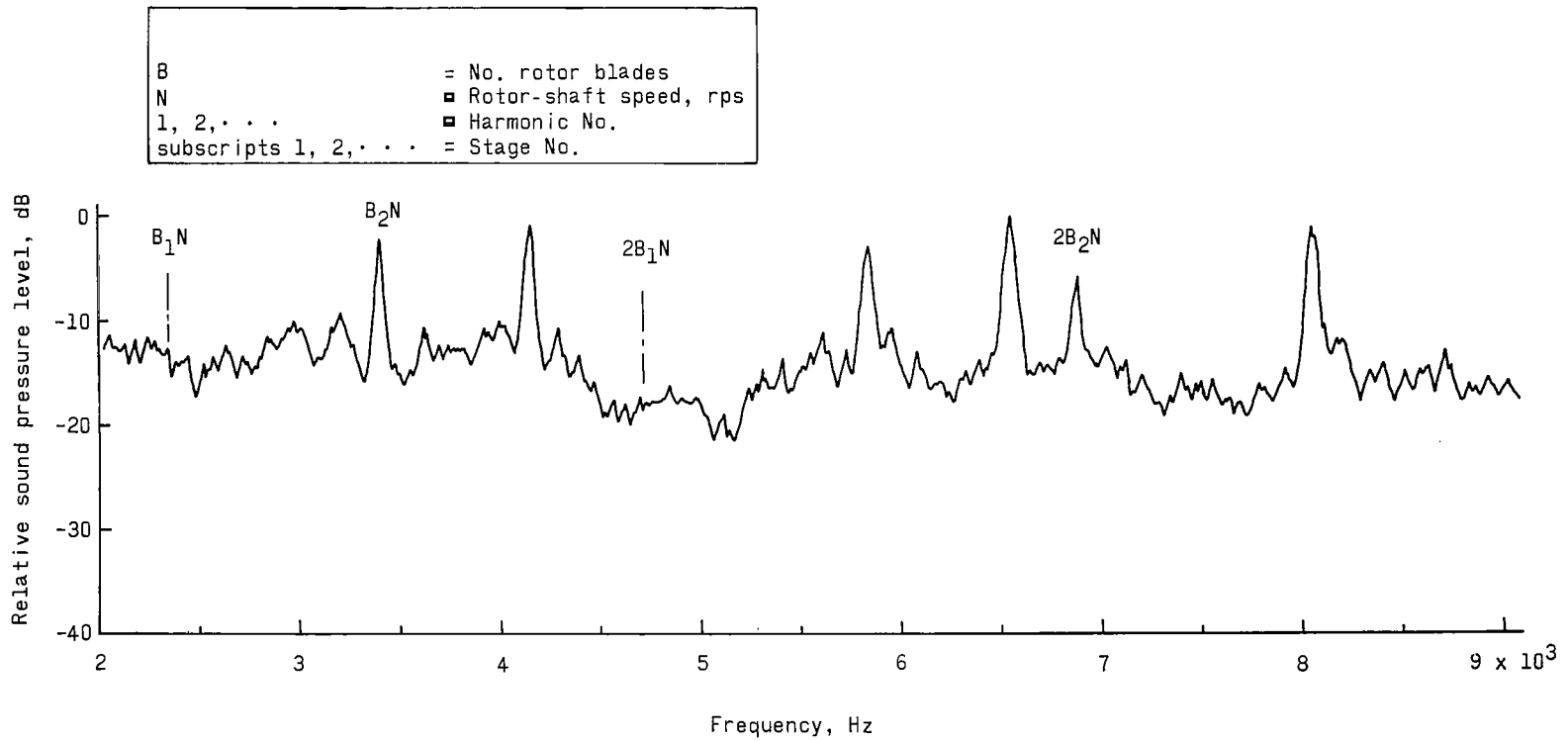
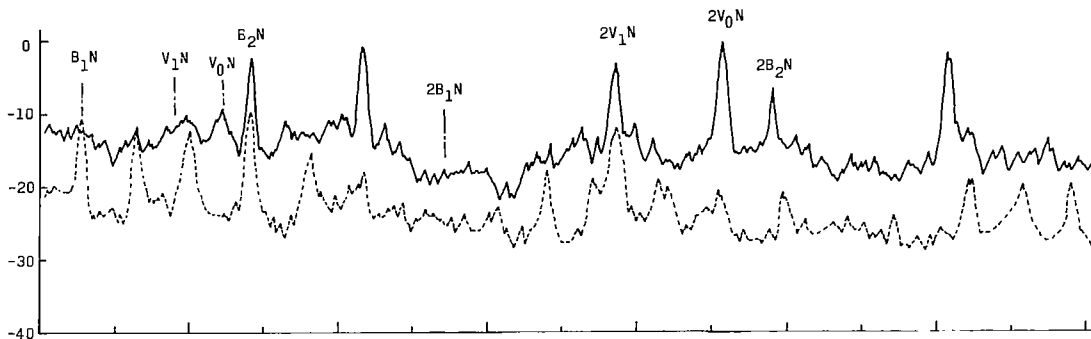
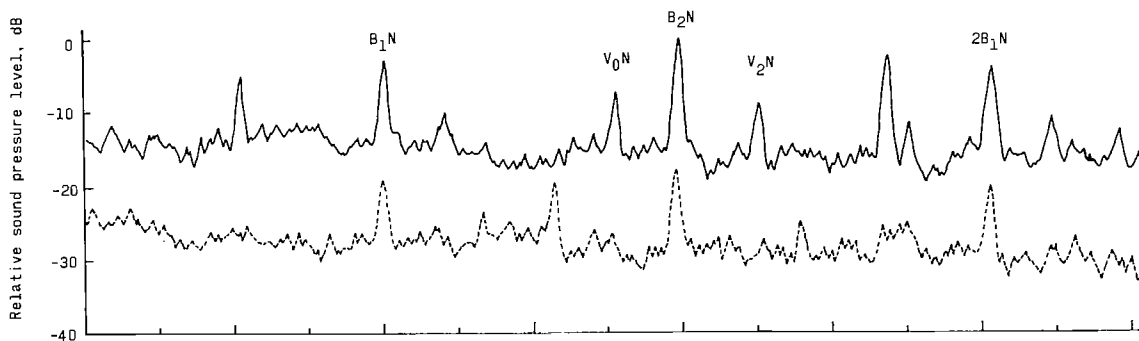


Figure 9.- Frequency analysis, using 50-hertz constant-bandwidth filter, for standard engine as measured at 30° azimuth location on a 25-foot (7.62-meter) radius for an engine speed of 35-percent rated rpm.

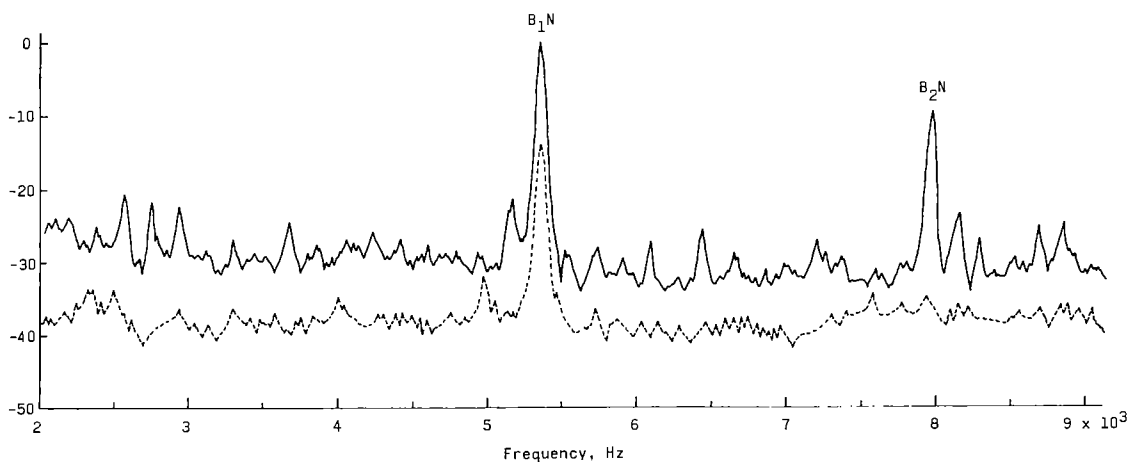
B	= No. rotor blades	
N	= Rotor shaft speed, rps	
V	= No. vanes	— Standard engine
1, 2, . . .	= Harmonic No.	- - - Modified engine
subscript 0	= Inlet guide vanes	
subscripts 1, 2, . . .	= Stage No.	



(a) 35-percent rated rpm.



(b) 60-percent rated rpm.



(c) 80-percent rated rpm.

Figure 10.- Frequency analysis, using 50-hertz constant-bandwidth filter, for standard and modified engine as measured at 30° azimuth location on a 25-foot (7.62-meter) radius for three engine speeds.